ELSEVIER

Automation in Construction 17 (2007) 3 – 10

AUTOMATION IN CONSTRUCTION

www.elsevier.com/locate/autcon

A UAV for bridge inspection: Visual servoing control law with orientation limits

Najib Metni [a,*], Tarek Hamel [b]

[a] *Laboratoire Centrale des Ponts et Chaussées, 58 bld Lefebure, 75732 Paris, France*
[b] *13S-CNRS, 2000 route des Lucioles, 06903 Sophia Antipolis, France*

Accepted 22 December 2006

Abstract

This paper describes the dynamics of an unmanned aerial vehicle (UAV) for monitoring of structures and maintenance of bridges. It presents a novel control law based on computer vision for quasi-stationary flights above a planar target. The first part of the UAV's mission is the navigation from an initial position to a final position in an unknown 3D environment. The new control law uses the homography matrix computed from the information obtained from the vision system. The control scheme will be derived with backstepping techniques. In order to keep the camera's field of view, the control law uses saturation functions for bounding the UAV orientation and limiting it to very small values.

Keywords: Bridge inspection; Visual servoing; Unmanned aerial vehicles; Automation

1. Introduction

Rapid advances in control theories, computing abilities, communications, and sensing technology offer a great tool for the unmanned aerial vehicles technology. In the last two decades a great interest in the UAV technology has risen in military applications, and many projects have been studied and applied.

In LCPC-Paris (Laboratoire Central des Ponts et Chaussées), we have started a project pertaining to civil applications of a UAV: bridge inspection and traffic surveillance. This project for bridges' inspection is called PMI (Plate-forme Mobile d'Instrumentation) which is a UAV capable of quasi-stationary flights whose mission is the inspection of bridges and location of defects and cracks.

Ageing infrastructure has become a major concern in western European countries. In France, roughly half of the bridge life cost is due to repairing and maintenance. Since many bridges were built in the sixties, health diagnostics and assessment of residual life already proves very important and will become increasingly crucial in the following decades. To this end, systematic bridge inspection has been organized for a long time and well-defined visual observation and reporting task are periodically carried out on bridges [1,2], this inspection must be done at least once every 6 years to control the evolution of defects and cracks. Current visual inspection involves a rather heavy logistics. A large platform mounted on a heavy truck is

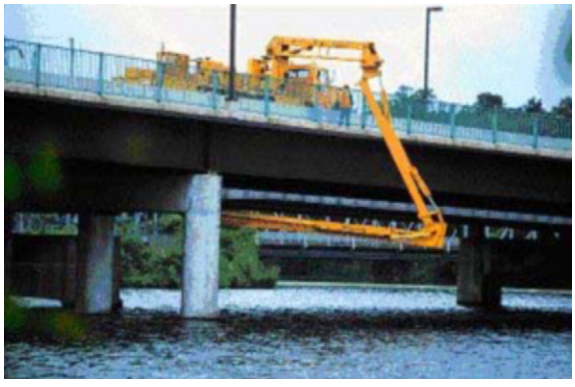

Fig. 1. Footbridge for crack's inspection.

* Corresponding author. Tel.: +33 1 40436510; fax: +33 1 40436513.
E-mail address: metni@lcpc.fr (N. Metni).

0926-5805/$ - see front matter © 2007 Elsevier B.V. All rights reserved.
doi:10.1016/j.autcon.2006.12.010

operated by a team of highly specialized inspectors, who work in extremely difficult and risky conditions, looking for small defects or damages in sometimes hardly accessible components of the structure (i.e. cables). Of course, the bridge under inspection is closed to traffic. This gives rise to a classical footbridge. Fig. 1 shows an example of a classical footbridge.

Progresses in visual bridge inspection look possible in the direction of remote sensing and process automating. The use of unmanned aerial vehicles could be of a particular interest as camera carriers and image transmitters. The UAV could follow a predetermined path or could move by visual servoing and detects by the means of image treatment the size and location of defects and cracks. The use of a drone for inspection will give us multiple advantages over traditional inspection method:

- Reducing work accident risk.
- Budget reduction: less logistics and less working hours.
- The bridge will ultimately not be closed for traffic.
- The possibility of using nondestructive techniques (infrared, shearography, …) for crack's detection.

For the sake of this application, a novel control law based on visual servoing is derived to control the UAV. Almost all control theories for UAV's are built around a vision system, using visual servoing as a control method. A typical vision system will include an off-the-shelf camera, Inertial Navigation System (INS) and in some cases a Global Positioning System (GPS).

In this paper, we consider a general mechanical model of a flying robot capable of quasi-stationary maneuvers. Then we derive a control law from classical backstepping techniques [3] of autonomous hovering system based on operating the translational from the rotational rigid body (airframe) dynamics. A novel approach is also presented; it will limit the orientation of the UAV. Limiting the orientation will ensure that the object will remain in the camera's field of view. We will prove the stability of such a strategy based on saturation functions. Lastly, we present some simulation results of the new control law and the feasibility trial executed on the viaduct of Saint Cloud in Paris.

2. Related work

The principal question that naturally arises while using vision in control application is:

How should the information from vision sensors be used for robotic control purposes?

There exist three different methods of visual servoing: 3D, 2D and 2½D. 3D visual servoing techniques that involve reconstruction of the target pose with respect to the camera are called: *position based visual servoing* (3D visual servoing). This kind of techniques leads to a Cartesian motion planning problem. Its main drawback is the need of a perfect knowledge of the target geometric model. The second class known as *image based visual servoing* (2D visual servoing) aims to control the dynamics of features in the image plane directly [4]. Classical 2D methods suffer from the high coupling dynamics between translation and rotational motion which makes the Cartesian trajectory uncontrollable. In this paper we use a third method presented in [5] (2½D visual servoing) that consists of combining visual features obtained directly from the image, and features expressed in the Euclidean space. More precisely, a homography matrix is estimated from the planar feature points extracted from the two images (corresponding to the current and desired poses). From the homography matrix, we will estimate the relative position of the two views.

3. A general UAV dynamic model

To derive a general dynamic model for a UAV is not an easy task because each model has its own capabilities and aerodynamical properties. In this section, we will derive mechanical equations for UAV's in hover or quasi-stationary conditions.

Let $F^* = \{E_x, E_y, E_z\}$ denote a right-hand inertial or world frame, such that E_z denotes the vertical direction downwards into the earth. Let $\xi = (x, y, z)$ denote the position of the center of mass of the object in the frame F^* relative to a fixed origin in F^*. Let $F = \{e_1, e_2, e_3\}$ be a (right-hand) body-fixed frame for the airframe. The orientation of the airframe is given by a rotation $R{:}F \rightarrow F^*$, where $R \in$ SO [3] is an orthogonal rotation matrix.

Let $V \in F$ denote the linear velocity and $\Omega \in F$ denote the angular velocity of the airframe both expressed in the body-fixed frame. Let m denote the mass of the rigid object and let $\mathbf{I} \in \Re^{3\times 3}$ be the constant inertia matrix around the center of mass (expressed in the body-fixed frame F). Newton's equations of motion yield the following dynamic model for the motion of a rigid object:

$$\dot{\xi} = RV \tag{1}$$

$$m\dot{V} = -m\Omega \times V + \mathcal{F} \tag{2}$$

$$\dot{R} = R\,\mathrm{sk}(\Omega), \tag{3}$$

$$\mathbf{I}\dot{\Omega} = -\Omega \times \mathbf{I}\Omega + \boldsymbol{\Gamma}. \tag{4}$$

where $\mathcal{F}$ is the vector forces and $\boldsymbol{\Gamma}$ is the vector torques. The notation sk (Ω) denotes the skew-symmetric matrix such that sk $(\Omega)\upsilon = \Omega \times \upsilon$ for the vector cross-product $\times$ and any vector $\upsilon \in \Re^3$. The vector force $\mathcal{F}$ is defined as follows:

$$\mathcal{F} = mgR^T e_3 - ue_3$$

In the above notation, g is the acceleration due to gravity, the u is the motor input force.

4. Camera modeling and visual servoing method

In this connection we will present a brief discussion of the camera projection model and then introduce the homography matrix to use the 2½D visual servoing method.

For the control law we will derive the error dynamics equations from Eqs.(1)–(4), they will be based on a defined visual error. Using the Lyapunov control design, we will find the desired force u and the desired orientation R_d to converge the UAV to a position described by a desired image.

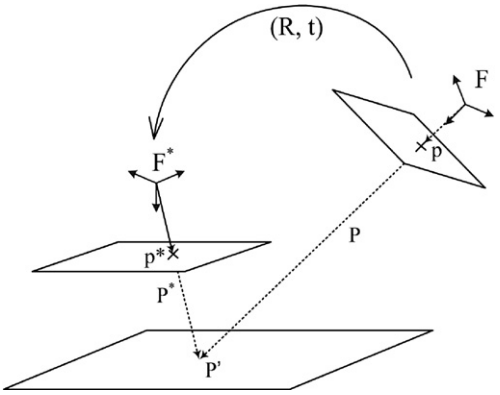

Fig. 2. Camera projection diagram showing the desired (F^*) and the current (F) frames.

4.1. Projection model and planar homography

Visual data is obtained via a projection of real world images onto the camera image surface. This projection is parameterized by two sets of parameters: intrinsic (i.e. those internal parameters of the camera such as the focal length, the pixel aspect ratio, etc.). The pose of the camera determines a rigid body transformation from the world or inertial frame F^* to the camera fixed frame F (and vice-versa). One has

$$P^* = RP + \xi \tag{5}$$

as a relation between the coordinates of the same point in the body-fixed frame ($P \in F$) and in the world frame ($P^* \in F^*$).

Let p is the image of the point P^* and p^* is the image of the same point viewed when the camera is aligned with frame F^* (see Fig. 2). When all target points lie in a single planar surface one has[1]

$$p_i \cong \left(R^T + \frac{tn^{*T}}{d^*}\right) p_i^*, \quad i = 1,\ldots,k$$

where t is the translation vector between the two frames F and F^*. d^* is the estimated distance between the desired image and the target. n^* being the normal vector to the desired image. The projective mapping $H := \left(R^T + \frac{tn^{*T}}{d^*}\right)$ is called a homography matrix; it relates the images of points on a target plane when viewed from two different poses (defined by the coordinate systems F and F^*). More details on the homography matrix could be found in [6]. The homography matrix contains the pose information (R,t) of the camera. However, since a projective relationship exists between the image points and the homography, it is only possible to determine H (using only image points equations) up to a scale factor. There are numerous approaches for determining H, up to this scale factor, for example [7].

Extracting R and t / d^* can be quite complex [5,8,9,10]. However, one quantity $r = \frac{d}{d^*}$ can be calculated easily and directly:

$$r = 1 + \frac{n^T t}{d^*} = \det(H) = \det\left(R^T + \frac{tn^{*T}}{d^*}\right).$$

There are special cases where it is relatively straight forward to compute important parameters from an unscaled estimate of the homography H. An important case is where the target plane is perpendicular to the line of sight of the world frame ($n^* + (0,0,1)^T$)). In this case, the first two columns of H are scaled versions of the first two columns of R. This special case is particularly useful while stabilizing the UAV in front of a planar area on the bridge to inspect closely some defects, the camera will be mounted so as its line of sight is perpendicular to the planar target. This case will be used in our simulation (Section 7).

4.2. Visual servoing control strategy

By exploiting Eqs.(1)–(4) and defining a visual error ϵ_1, in this section we derive the error dynamics equations and by using the Lyapunov functions, we find the desired control input (force and orientation) u and R_d.

To simplify the derivation, it is assumed that the camera fixed frame coincides with the body-fixed frame F.

Let P' denote the observed point of reference of the planar target, and P^* be the representation of P' in the camera fixed frame at the desired position (Fig. 2). The dynamics associated with the stabilization of the camera around the desired position P^* fully determine two degrees of freedom (pitch and roll) in the attitude of the airframe. The yaw angle trajectory is specified directly in terms of the desired yaw angle ϕ_d. In this paper, to determine the rotation matrix we use the classical 'yaw', 'pitch' and 'roll' Euler angles (ϕ, θ, ψ) commonly used in aerodynamic applications [11]. The expression of the rotation matrix is given by:[2]

$$R = \begin{pmatrix} c_\theta c_\phi & s_\psi s_\theta c_\phi - c_\psi s_\phi & c_\psi s_\theta c_\phi + s_\psi s_\phi \\ c_\theta s_\phi & s_\psi s_\theta s_\phi + c_\psi s_\phi & c_\psi s_\theta s_\phi - s_\psi c_\phi \\ -s_\theta & s_\psi c_\theta & c_\psi c_\theta \end{pmatrix}. \tag{6}$$

The visual servoing problem considered is:

Find a smooth force feedback u depending only on the measurable states: the observed point p, the homography matrix H, the translational and angular velocities (V, Ω), and the estimated parameters (R, r) from the homography matrix (H) which provide a partial pose estimation, such that the following errors

$$\epsilon = R\left(P - R^T P^*\right), \quad \sigma = \phi - \phi d$$

are asymptotically stable.

[1] Most statements in projective geometry involve equality up to a multiplicative constant denoted by $\cong$.

[2] The following shorthand notation for trigonometric function is used:

$c_\beta := \cos(\beta)$, $s_\beta := \sin(\beta)$, $t_\beta := \tan(\beta)$.

Note: ϵ and σ are not defined in terms of visual information.

Following [5], the camera can be controlled in the image space and in the Cartesian space at the same time. They propose the use of three independent visual features, such as the image coordinates of the target point associated with the ratio r delivered by the determinant of the homography matrix. Consequently, let us consider the reference point P' lying in the reference plan π and define the scaled Cartesian coordinates using visual information as follow:

$$P_r = \frac{n^{*T}p^*}{n^T p} rp.$$

Knowing that

$$\frac{||P||}{||P^*||} = \frac{n^{*T}p^*}{n^T p} r,$$

it follows that we can reformulate the error ϵ in terms of available information, so let us define

$$\epsilon = R\left(\frac{n^{*T}p^*}{n^T p} rp - R^T p^*\right). \tag{7}$$

From the above discussion and equations describing the system dynamics, the full dynamics of the error ϵ may be written as

$$\dot{\epsilon} = \frac{1}{||P^*||}\upsilon \tag{8}$$

$$m\dot{\upsilon} = -uRe_3 + mge_3 \tag{9}$$

$$\dot{R} = R\mathrm{sk}(\Omega) \tag{10}$$

$$\mathbf{I}\dot{\Omega} = -\Omega \times \mathbf{I}\Omega + \boldsymbol{\Gamma}. \tag{11}$$

Define

$$\delta := \epsilon + \upsilon. \tag{12}$$

Let S_1 be the first storage function for the backsteeping procedure. It is chosen for the full linear dynamics Eqs.(8) and (9)

$$S_1 = \frac{1}{2}||\delta||^2 + \frac{1}{2}||\upsilon||^2. \tag{13}$$

Taking the time derivative of S_1 and substituting for Eqs.(8) and (9) yield

$$\frac{d}{dt}S_1 = \rho\delta^T\upsilon + (\delta+\upsilon)^T(mge_3 - uRe_3) \tag{14}$$

where $\rho = \frac{1}{||P^*||}$. This inverse distance ρ cannot be found or identified, so we will test its identifiability as an unknown parameter in Appendix A.

Applying classical backstepping one would assign a virtual vectorial control for $\frac{1}{m}(uRe_3)^d$

$$u(Re_3)^d = mge_3 + m\upsilon + m\delta. \tag{15}$$

This choice is sufficient to stabilize S_1 if the term $(uRe_3)^d$ is available as a control input. If $(uRe_3)=(uRe_3)^d$ then

$$\dot{S}_1 = -||\delta||^2 - (2-\rho)\delta^T\upsilon - ||\upsilon||^2$$

is a negative definite $\forall\rho<1$.[3]

Note that the vectorial input can be split into its magnitude u, that is linked directly to the motor torques, and its virtual (or desired) direction $(R_\mathrm{d}e_3)$, that defines two degrees of freedom in the airframe attitude dynamics (Eqs.(10) and (11)):

$$|u| = mge_3 + m\upsilon + m\delta||$$

and the desired direction

$$R_\mathrm{d}e_3 = \frac{mge_3 + m\upsilon + \delta}{|u|}. \tag{16}$$

Now, to determine the fully desired rotation matrix R_d we had to find the constraint of the yaw parameter using another vector. Let e_1 be the desired orientation. We define the vector σ which belongs to the plane built by the two vectors e_1 and $R_\mathrm{d}e_3$ ($\sigma \in \mathrm{span}\{R_\mathrm{d}e_3, e_1\}$) and we impose that $\sigma = R_\mathrm{d}e_1$ (by this way, σ will be perpendicular to $R_\mathrm{d}e_3$). We obtain

$$\sigma = \frac{e_1 + \alpha R_\mathrm{d}e_3}{||e_1 + \alpha R_\mathrm{d}e_3||}; \quad \text{with } \sigma^T R_\mathrm{d}e_3 = 0. \tag{17}$$

Here α is a real number obtained by solving the two above equations. The final equation for the desired matrix R_d can be defined as:

$$R_\mathrm{d} = [\sigma \quad \sigma\wedge(R_\mathrm{d}e_3) \quad R_\mathrm{d}e_3]. \tag{18}$$

The desired rotation matrix R_d in Eq.(18) is not subject to any restrictions. In the next section, the orientation will be limited to small values of the Euler angles.

5. Limiting the UAV orientation

In the theoretical developments based on the backstepping [3], the proposed control law assures an exponential convergence towards the desired position. However, this type of convergence is not recommended when the vehicle is initially far from the desired position. Indeed, the dynamic model based on quasi-stationary conditions (hovering conditions) is not valid anymore, because the dynamics of such a convergence will provoke a different flight mode. Moreover, the target image may leave the field of view of the camera during the evolution of the vehicle. To avoid such situations, it is necessary to insure that the focal axis of the camera is close to the gravity direction. In the sequel, we proposed to use small gains technique (for example the technique of saturation functions presented by Teel in [12]). This technique seems well adapted to our problem. Indeed, if the orientation is saturated, we can insure that the

[3] It is a significant condition because the distance P^* must be greater than 1 which is the focal length of the camera.

robot will remain in quasi-stationary maneuvers during all the operation.

The orientation $R_d e_3$ is a function of the terms υ and δ. Therefore, Eq.(15) becomes

$$uR_d e_3 = mge_3 + m\mathrm{Sat}_2(\upsilon + \mathrm{Sat}_1(\delta)) \tag{19}$$

where $\mathrm{Sat}_i(x)$ is a continuous, nondecreasing saturation function satisfying:

- $x^T \mathrm{Sat}_i(x) > 0$ for all $x \neq 0$.
- $\mathrm{Sat}_i(x) = x$ when the components of the vector x are smaller than L_i ($|x_{(\cdot)}| \leq L_i$).
- $|\mathrm{Sat}_i(x)| \leq M_i$ for all $x \in \mathbb{R}$.

Proposition 5.1. *The following choice of the saturation functions* [12]

$$M_i < \frac{1}{2}L_{i+1}; \quad \frac{1-\rho}{2}L_{i+1} \leq L_i \leq M_i$$

ensures global stabilization of the linear dynamics when Eq. (19) *is used as control input of the translational dynamics.*

Proof. Recalling Eqs.(9) and (19), it yields

$$\dot{\upsilon} = -\mathrm{Sat}_2(\upsilon + \mathrm{Sat}_1(\delta)).$$

Consider the storage function $S_\upsilon = 1/2\|\upsilon\|^2$. The derivative of S_υ is given by

$$\dot{S}_\upsilon = -\upsilon^T \mathrm{Sat}_2(\upsilon + \mathrm{Sat}_1(\delta)).$$

Using conditions on Sat_i coupled with the fact that $M_1 \leq L_2$, it follows that $\dot{S}_\upsilon < 0$ ($\forall |\upsilon_{(\cdot)}| \geq 1/2\ L_2$) ($\upsilon_{(\cdot)}$ represents a component of the vector υ). Consequently, it exists a finite time T_1 after which all components of the linear velocity vector $\upsilon_{(\cdot)} \leq 1/2\ L_2$ ($\forall t \geq T_1$). The control law Eq.(19) becomes then

$$u_4 R_d e_3 = mge_3 + m(\upsilon + \mathrm{Sat}_1(\delta)), \qquad \forall t \geq T_1.$$

Now consider the evolution of the term δ for $t \geq T_1$. Let S_δ the storage function associated with the term δ ($S_\delta = 1/2\|\delta\|^2$). Deriving S_δ it yields

$$\dot{S}_\delta = \delta^T((\rho - 1)\upsilon - \mathrm{Sat}_1(\delta)).$$

Using the second condition of the proposition, one can observe that the components of the vector δ become smaller than M_1 after a finite time T_2 where the control law becomes

$$uR_d e_3 = mge_3 + m(\upsilon + \delta), \qquad \forall t \geq T_2$$

insuring exponential stability after time T_2. □

Using the saturated control law (Eq.(19)), the derivative of the first storage function becomes

$$\dot{S}_1 = -\|\delta\|^2 - (2-\rho)\delta^T\upsilon - \|\upsilon\|^2 - (\delta + \upsilon)^T |u|^s \left(\tilde{R} - I\right) R_d e_3$$

where

$$\tilde{R} = RR_d^T; \text{ and } |u|^s = \|mge_3 + m\mathrm{Sat}_2(\upsilon + \mathrm{Sat}_1(\delta))\|.$$

According to the above proposition, the system with such a saturated input is globally asymptotically stable if the new error term $\tilde{R} - I$ converges to zero. Now, it only remains to control the attitude dynamics involving the error $\tilde{R} - I$.

6. Attitude dynamics control

The next step of the control design involves the control of the attitude dynamics such that the error $\tilde{R} - I$ converges exponentially to zero. We will use a quaternion representation of the rotation to obtain a smooth control for $\tilde{R}$. The attitude deviation $\tilde{R}$ is parameterized by a rotation $\tilde{\gamma}$ around the unit vector $\tilde{k}$ Using Rodrigues' formula [11] one has

$$\tilde{\mathrm{R}} = I + \sin(\tilde{\gamma})\mathrm{sk}\left(\tilde{\mathrm{k}}\right) + (1 - \cos\left(\tilde{\gamma}\right))\mathrm{sk}\left(\tilde{\mathrm{k}}\right)^2.$$

The quaternion representation describing the deviation $\tilde{R}$ is given by [13]

$$\tilde{\eta} := \sin\frac{\tilde{\gamma}}{2}\tilde{\mathrm{k}}, \quad \tilde{\eta}_d = \cos\frac{\tilde{\gamma}}{2}; \quad \text{with} \quad \|\tilde{\eta}\|^2 + \tilde{\eta}_0^2 = 1.$$

The deviation matrix $\tilde{R}$ is then defined as follows

$$\tilde{R} = \left(\tilde{\eta}_0^2 - \|\tilde{\eta}\|^2\right) I + 2\tilde{\eta}\tilde{\eta}^T + 2\tilde{\eta}_0 \mathrm{sk}(\tilde{\eta}). \tag{20}$$

The attitude control objective is achieved when $\tilde{R} = I$. From Eq.(20) this is equivalent to $\eta = 0$ and $\tilde{\eta}_0 = 1$. Indeed, it may be verified that

$$\|\tilde{R} - I\|_F = \sqrt{tr\left((R-I)^T\left(\tilde{R} - I\right)\right)} = 2\sqrt{2|\tilde{\eta}|}. \tag{21}$$

Based on this result, the attitude control objective is to drive $\tilde{\eta}$ to zero. Differentiating $(\tilde{\eta}, \tilde{\eta}_0)$ yields

$$\dot{\tilde{\eta}} = \frac{1}{2}(\tilde{\eta}_0 I + \mathrm{sk}(\tilde{\eta}))\tilde{\Omega}, \qquad \dot{\tilde{\eta}}_0 = -\frac{1}{2}\tilde{\eta}^T\tilde{\Omega}. \tag{22}$$

where $\tilde{\Omega}$ denotes the error angular velocity

$$\tilde{\Omega} = R_d(\Omega - \Omega_d) \tag{23}$$

and Ω_d represents the desired angular velocity. In order to find the desired angular velocity, we have to consider the time derivative of the desired orientation $R_d e_3$

$$\dot{R}_d = R_d \mathrm{sk}(\Omega_d); \quad \dot{R}_d e_3 = R_d e_3 \mathrm{sk}(\Omega_d). \tag{24}$$

Since differentiating the direction $R_d e_3$ involves the use of the unknown parameter ρ which is nonidentifiable (Appendix

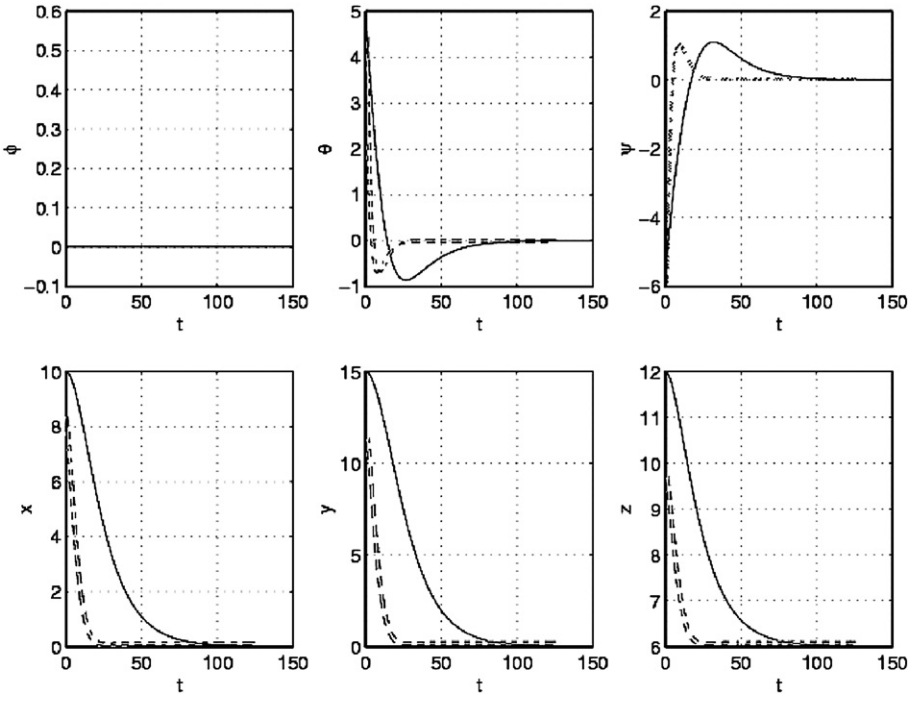

Fig. 3. Evolution of the "X4-flyer" states (the 3 Euler Angles [radian] and the 3 coordinates [meter]) in the 2 control laws; without limiting its orientation (dashed lines—angles in 10^{-1} rad), and the new control law (full lines—angles in 10^{-3} rad).

A), we will design a control law with a high gain virtual control $\tilde{\Omega}^v$. In this way we can neglect the effect of the time derivative of $R_d e_3$.

Then, by choosing the virtual control as

$$\tilde{\Omega}^v \approx \Omega^v = -2k\tilde{\eta}_0\tilde{\eta}$$

with the parameter k chosen high enough to neglect Ω_d. Let

$$v = \frac{1}{k}\Omega + R_d^T\tilde{\eta}_0\tilde{\eta}. \tag{25}$$

After tedious calculations, we obtain the time derivative of v

$$\dot{v} = -\frac{k}{2}\tilde{\eta}_0 R_d^T\tilde{\eta} - \frac{k}{2}||\tilde{\eta}_0||^2 v. \tag{26}$$

Let us define the Lyapunov function candidate for the attitude deviation:

$$S_2 = \frac{1}{2}||\tilde{\eta}||^2 + \frac{1}{2}||v||^2. \tag{27}$$

Taking the time derivative of S_2 and using Eq.(26), we obtain

$$\dot{S}_2 = -\frac{k}{2}||\tilde{\eta}_0||^2||\tilde{\eta}||^2 - \frac{k}{2}||\tilde{\eta}_0||^2||\tilde{v}||^2. \tag{28}$$

This completes the control design for the attitude dynamics, since the time derivative of the storage function in Eq.(28) is a negative definite. Then the input of the new control law (Eq.(19)) limiting the orientation ensures the exponential stability of the system.

7. Simulation results

In order to evaluate the efficiency of the proposed servoing technique with orientation limits, simulation results for a hovering robot are presented. The experiment considers a basic stabilization mission. The target is composed of five points: four on the vertices of a planar square and one on its center. The available signals are the pixel coordinates of the five points observed by the camera.

For this experiment, it is assumed that the desired plane is perpendicular to the line of sight. The desired image feature is chosen such that the camera set point is located some meters above the square.

The parameters used for the dynamical model are m=0.6, I=diag[0.4, 0.4, 0.6], g=10, d=0.25 and κ=0.01. Initially, the robot is assumed to hover at (10,15, −12) with thrusts

Fig. 4. Photo taken front the feasibility test done on the viaduct of Saint Cloud.

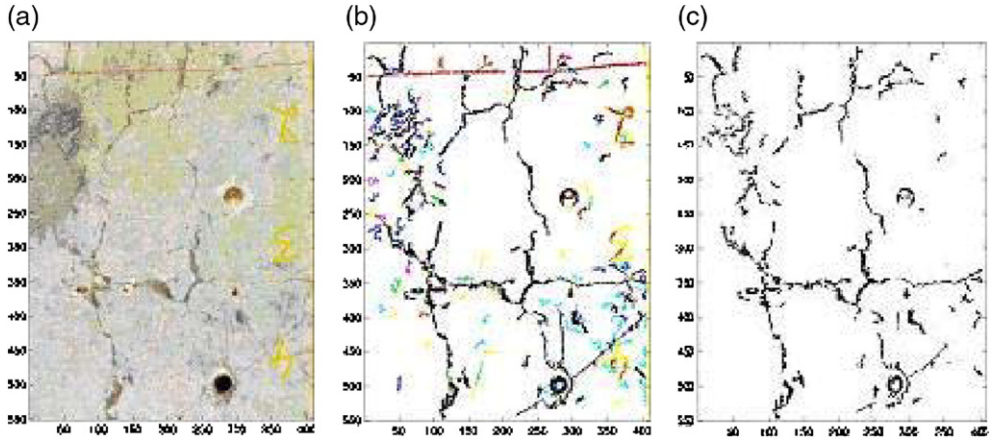

Fig. 5. In (a) the image is coded in RGB. It is then compared to a threshold value for each color layer in (b). In (c) we insulate black pixels corresponding to cracks.

corresponding the necessary forces to maintain stationary flight $u_4 \approx mg$.

We will compare the results of the new control law (with orientation limits) versus the evolution of the states in the control law (without orientation limits) developed in [6]. One can notice (Fig. 3) that the time of convergence for the states following the new law of control is longer than the previous law, but instead we see that the variation of the Euler angles are restricted to small values (in this case, in order of 10^{-3} rad). So the new control law which limits the X4-flyer orientation ensures small values of the Euler angles, therefore we insure that the dynamics of the flying vehicle are applicable to the hover conditions (quasi-stationary maneuvers) and the object will remain in the field of view of the camera.

7.1. Feasibility experiment: viaduct of Saint Cloud

In order to validate the concept of inspecting bridge defects by means of a visual device mounted on a UAV, an on-site experiment has been carried out with the help of a helicopter that has been flying few minutes around a viaduct in France, then taking a video from which some pictures have been extracted (Fig. 4). It was also a test for the required security measures and applicable regulations. The choice of this particular viaduct was made due to its morphology and situation. This viaduct with particularly high traffic is located indeed in an urbanized zone subjected to the control of two airports. It is constructed above the "Seine" and connecting two cities: Boulogne-Billancourt and Saint Cloud, which will make the prerequisite authorizations a more complex task.

During the test, a video sequence was taken using the onboard camera. The images were presented to bridge inspection experts to analyze them. The exploitation of the images demonstrates the possibility of getting useful information comparing to visual inspection. Additional image treatment with good image resolution will let us detect cracks of the order of 1/10 mm (Fig. 5).

8. Conclusion

This paper reflects a control law of a UAV under some practical restrictions. It presents a control strategy for the autonomous flight with orientation limits in order to keep the object in the camera's view field. This strategy only requires that the system is able to measure, with a video camera, the image plane mapping features on a planar surface. A control law based on separating translation and orientation dynamics is exploited. It also limits the UAV's orientation to small values of angles while stabilizing it above a planar target.

Appendix A. Test for the identifiability of ρ

In this appendix, we will apply the conditions given by [14] to test the identifiability of the parameter ρ. The test is known as the *generating series test*; it is based on power series associated with the system. Rewriting the system Eqs.(8)–(11) using the notation $x_1=\epsilon_1$, $x_2=v$, $x_3=R$, and $x_4=\Omega$:

$$\dot{x} = f_0(x,\rho) + f_1(x,\rho)u + f_2(x,\rho)\boldsymbol{\Gamma} \tag{29}$$

where

$$f_0 = \begin{bmatrix} 0 & \rho x_2 & 0 & 0 \\ 0 & 0 & 0 & 0 \\ 0 & 0 & x_3 \mathrm{sk}(x_4) & 0 \\ 0 & 0 & 0 & -\mathbf{I}^{-1}x_4 \times \mathbf{I}x_4 \end{bmatrix}$$

$$f_1 = \begin{bmatrix} 0 \\ -\dfrac{1}{m}ux_3e_3 \\ 0 \\ 0 \end{bmatrix} \qquad f_2 \begin{bmatrix} 0 \\ 0 \\ 0 \\ \mathrm{I}^{-1} \end{bmatrix}.$$

To simplify the test, we eliminate the term ge_3 from the equation. This elimination won't alter in any way the result of this test. Let us consider the vector fields associated with the last system:

$$\begin{aligned} F_0(x,\rho)[.] &= \rho x_2 \frac{\partial}{\partial x_1} + [x_3 \ \mathrm{sk}(x_4)] \frac{\partial}{\partial x_3} - \left[\mathbf{I}^{-1}x_4 \times \mathbf{I}x_4\right] \frac{\partial}{\partial x_4} \\ F_1(x)[.] &= \frac{1}{m}x_3e_3 \frac{\partial}{\partial x_3} \\ F_2(x)[.] &= \mathrm{I}^{-1} \frac{\partial}{\partial x_4} \end{aligned}$$

Then we compute the Lie derivatives of any output function y and evaluate it at $x=x^*$ where $x_1=x_2=x_4=0$, $x_3=I$: $F_1(F_0(x^*, \rho)[y])$, $F_2(F_0(x^*,\rho)[y])$, $F_2(F_0(F_0(x^*,\rho)[y]))$. The parameter will be identifiable if the system has a unique solution for ρ. In our case, the Lie derivatives all vanish at $x=x^*$ so the system is structurally nonidentifiable.

Appendix B. Glossary of symbols

$F^*=\{E_x, E_y, E_z\}$ Right handed inertial (world) frame.
$F=\{e_1, e_2, e_3\}$ Right handed body-fixed frame.
$\xi=(x, y, z)$ Position of the center of mass.
$R:F\rightarrow F^*$ Orthogonal rotation matrix.
R_d Desires orientation matrix.
$\tilde{R}$ Deviation (error) between R and R_d.
V Linear velocity of the mobile expressed in F^*.
υ Linear velocity of the mobile expressed in F.
Ω Angular velocity of the mobile expressed in F.
$\mathbf{I}$ Constant Inertia matrix around the center of mass.
$\mathcal{F}$ Vector of external forces applied to the mobile.
$\mathbf{\Gamma}$ Vector of external torques applied to the mobile.
u Motor input force due to rotors.
P^* Point expressed in F^*.
P P^* expressed in F.
t Translation vector between the two frames F and F^*.
d^* Distance between the desired image and the target.
ρ Inverse of the distance d^*.
n^* Normal vector to the desired image.
H Homography matrix.
(ϕ, θ, ψ) Euler angles used in aerodynamic application.
δ Error defined in terms of visual information.
M_i, L_i Properties of the saturation functions.
$(\tilde{\eta},\tilde{\eta}_0)$ Quaternions describing the deviation $\tilde{R}$

References

[1] B. Godart, La surveillance renforcée et la haute surveillance des ouvrages d'art en france, Bulletin du Laboratoire Central des Ponts et Chaussées, vol. 227, LCPC, 2000.
[2] Instruction technique pour la surveillance et l'entretien des ouvrages d'art, Documents edited and diffused by the lcpc and setra, 1991.
[3] T. Hamel, R. Mahony, Visual servoing of under-actuated dynamic rigid body system: An image space approach, 39th Conference on Decision and Control, 2000.
[4] S. Hutchinson, D. Hager, P. Cake, A tutorial on visual servocontrol, IEEE Trans. Robot. Autom. 12 (1996).
[5] E. Malis, Contribution à la modélisation et à la commande en asservissement visuel, Ph.D. thesis, Université de Rennes (1998).
[6] D. Suter, T. Hamel, R. Mahony, Visual Servoing Based on Homography Estimation for the Stabilization of an X4-flyer, 2002.
[7] B. Couapel, B. Bainian, Stereo vision with the use of a virtual plane in the space, Chin. J. Electron. 4 (2) (1995) 32–39.
[8] Z. Zhang, A. Hanson, Scaled Euclidean 3D reconstruction based on externally uncalibrated cameras, IEEE symposium on Computer Vision. Coral Glabes, Floride, 1995.
[9] J. Weng, T. Huang, N. Ahuja, Motion and Structure from line Correspondences: Closed-form Solution, Uniqueness, and Optimization, 1992.
[10] O. Faugeras, F. Lustman, Motion ans structure from motion in a piecewise planar environment, Int. J. Pattern Recogn. Artif. Intell. 2 (3) (1998) 485–508.
[11] R. Murray, Z. Li, S. Sastry, A Mathematical Introduction to Robotic Manipulation, CRC Press, 1994.
[12] A. Teel, Global stabilization and restricted tracking for multiple integrators with bounded controls, Syst. Control. Lett. 18 (1992) 165–171.
[13] O. Egeland, M. Dalsmo, O. Sordalen, Feedback control of a nonholonomic underwater vehicle with constant desired configuration, Int. J. Robot. Res. 15 (1996) 24–35.
[14] Y. Lecourtier, F. Lamnabhi-Lagarrigue, Identifiability of Parametric Models, Pergamon Press, 1987.